文章编号：1001－9014(2018)02－0129－06

DOI:10.11972/j.issn.1001－9014.2018.02.001

# Understanding ferromagnetism in Carbon-doped rutile $TiO_2$ : first-principles calculations

HUANG Wen-Chao[1], WANG Xiao-Fang[1*], CHEN Xiao-Shuang[1*], LU Wei[1], FONG Ching-Yao[2]

(1. National Laboratory for Infrared Physics, Shanghai Institute of Technical Physics, Chinese Academy of Sciences, Shanghai 200083, China;
2. Department of Physics, University of California, Davis, CA 95616-8677, USA)

**Abstract**: First-principles calculations based on density functional theory have been performed on the nonmagnetic 2*p* light element carbon-doped rutile $TiO_2$, which is very appealing for spintronics and infranics. The results show that carbon dopants tend to couple ferromagnetically around the Ti atom in the rutile structure, and the magnetic moment per C is about 1.3 $\mu_B$. The ferromagnetism is predicted to be the collective effects from a *p-d* exchange hybridization and a *p-d* exchange-like *p-p* coupling interaction, between the impurity (*p*-like $t_{2g}$) and valence (*p*) states.

**Key words**: first principles, ferromagnetism, *p-p* coupling, half-metallicity
**PACS**: 75.70.Cn, 75.50.Pp, 75.30.-m, 72.80.Ey

# C 掺杂金红石结构 $TiO_2$ 的第一性原理研究

黄文超[1], 王晓芳[1*], 陈效双[1*], 陆 卫[1], 方敬尧[2]

(1. 中国科学院上海技术物理研究所 红外物理国家重点实验室,上海 200083;
2. 美国加利福尼亚大学物理系 戴维斯分校, CA 95616-8677)

**摘要**:利用基于密度泛函的第一性原理研究了非磁性轻元素 C 掺杂金红石 $TiO_2$ 的性质,这在自旋电子和红外电子领域具有潜在的应用前景.结果显示:C 原子更倾向于形成铁磁耦合并围绕在 Ti 原子周围,每个 C 原子的磁矩大约为 1.3 $\mu_B$.体系的铁磁性来源于 *p-d* 轨道杂化和类 *p-d* 杂化的 *p-p* 耦合共同作用,*p-p* 耦合主要来自类 *p*-$t_{2g}$和价带 *p* 态耦合.

**关 键 词**:第一性原理;铁磁性;*p-p* 耦合;半金属

**中图分类号**:O441.2,O482.52,O482.54　　**文献标识码**:A

## Introduction

To incorporate additional components in $TiO_2$ structure, there are mainly two ways which is metallic or non-metallic doping. However, there are some disadvantages of metallic doping, such as poor thermal stability, photo-corrosion, and being recombination centers. By contrast, non-metal (C, B, F, N, etc.) doping is far more successful than metal doping in shifting the ultraviolet to the visible light range.

Doped with transition metals, $TiO_2$ becomes the important diluted magnetic semiconductors (DMSs), which is very appealing for spintronics and infranics[1-9]. In this rapidly developing research area, the spin functionality can be integrated into the usual charge degree of freedom so that the novel properties can be used in many infrared electronic devices to improve functional performances. However, the ferromagnetic (FM) semiconductors are required to have a high Curie temperature ($T_C$) for the applications at room temperature. To date, many efforts have been devoted to this goal in oxide semiconductors, such as magnetic ion Ti, V, Cr, Mn, Fe, Co, and Ni doped ZnO, $TiO_2$, $SnO_2$, $In_2O_3$, and $HfO_2$ materials[1-11], which are candidates for room temperature (RT) DMSs with highly potential industrial applications

**Received date**: 2015-01-04, **revised date**: 2015-11-03　　**收稿日期**:2015-01-04, **修回日期**:2015-11-03
**Foundation items**:Supported by National Natural Science Foundation of China (11104299, 61006090), the Fund of Shanghai Science and Technology Foundation (16ZR1447400)
**Biography**:HUANG Wen-Chao(1985-), Lanzhou, doctor, he is devoted to the study of magnetics with first-principles. E-mail:: wchuang@mail.sitp.ac.cn
* **Corresponding author**:E-mail:wxiaof66@mail.sitp.ac.cn, xschen@mail.sitp.ac.cn

in spintronics and infranics. Among them, $TiO_2$-based DMSs, as a wide band gap semiconductor, have attracted much attention through their additional application in various areas[12-21] including photocatalysis, infrared response, infrared electronic devices and sensors. The rutile $TiO_2$ has high static dielectric constants (86-170), which makes it a candidate for replacing $SiO_2$ as the gate material of the future. However, the sample growth is very sensitive to the preparation methods and conditions, making the experimental results quite controversial[7, 9]. One of the fundamental and key questions is whether the grown material is indeed a solid solution of $Ti_{1-x}TM_xO_2$ (TM = V, Cr, Mn, Fe, Co, etc.), or it remains as $TiO_2$ with embedded TM clusters, precipitates, or second phases, responsible for the observed magnetic properties. A possible way to avoid this problem is to dope $TiO_2$ with nonmagnetic elements[22]. In fact, the theoretical studies have predicted that anion substitutions in IIA-oxide can also lead to FM, but the mechanism will be very different compared to that of the cationic impurities[23]. The anionic impurities contain only *sp* electrons, which provide a new concept in the developments for potentially useful DMSs.

The most recent attractive results that RT FM with $T_C$ higher than 400 K was observed in C-doped ZnO have drawn our attention[24-25]. Pan *et al* theoretically reported the FM coupling among the C dopants and a magnetic moment of 2.02 $\mu_B$ per C. The result was confirmed experimentally by pulsed-laser deposition with dpoing concentration around 2.5%. They attributed the FM to a *p-d* exchange-like *p-p* coupling interaction, derived from the similar symmetry and wave function between the impurity (*p*-like $t_{2g}$) and valence (*p*) states. Yu *et al.* reported the FM in N-embedded ZnO: N films[26]. Bannikov *et al.* reported the spin polarization induced by replacement of O atoms by nonmagnetic 2*p* impurities (B, C and N) in nonmagnetic cubic $SrMO_3$ (M = Ti, Zr and Sn) perovskite, and the FM appears because of the spin-split impurity bands inside the energy gap of the insulating $SrMO_3$ matrix[27]. Wu *et al.* found that C substitution for either single B or N atom in the BN nanotubes can induce spontaneous magnetization[28]. Furthermore, the C system itself is intriguing from a fundamental scientific point of view[29]. Another words, it is an interesting and physically rich topic to study the magnetic properties of the C-doped $TiO_2$ without resorting to magnetic ions.

In this paper, we present a systematic first-principles study of the electronic and magnetic properties in C-doped rutile $TiO_2$. We focus on the possibility of the magnetization for $TiO_2$ induced by nonmagnetic *sp* impurities.

## 1 Method of calculation

$TiO_2$ has three possible structures: rutile, anatase, and brookite, with rutile being the most thermodynamically stable. Thus, we chose the rutile structure. The geometric details of the used supercell can be found in Fig. 1, where a supercell consisting of $2\times2\times2$ periodic repetition of the primitive unit cell is constructed. Calculations of the total energies, forces, and optimizations of geometry have been carried out using a plane-wave basis set with the pseudopotentials determined by the projector augmented plane-wave (PAW) method[30] as implemented in the Vienna *ab initio* simulation package (VASP)[31]. The generalized-gradient approximation (GGA) is employed for treating the exchange and correlation potential[32]. The summation over the irreducible Brillouin zone is carried out with *k*-points sampling including Γ point based on the Monkhorst-Pack grid[33], with parameters of $4\times4\times6$ grid. The plane-wave energy cutoff is set to 500 eV. All the atoms and internal coordinates are allowed to relax without any symmetry constraint. The ionic relaxation to the equilibrium structure is determined using a conjugate-gradient algorithm, and the convergence in energy and force are $1.0\times10^{-4}$ eV and $1.0\times10^{-2}$ eV/Å, respectively.

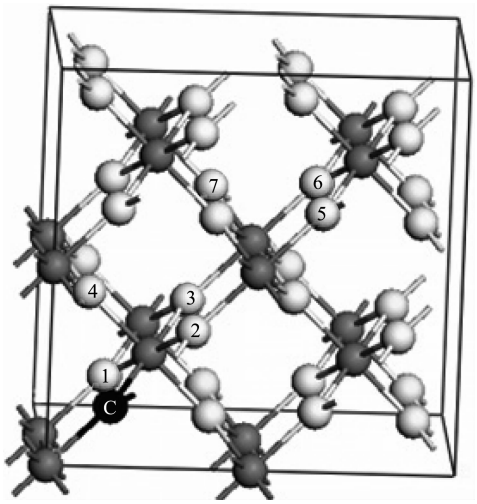


Fig. 1 The periodic supercells modeling the $2\times2\times2$ C-doped rutile $TiO_2$ structure. The gray, white and black spheres represent Ti, O and C atoms, respectively. The numbers 1-7 denote the possible C sites, which consider seven different relative C-C configurations

图1 C掺杂金红石 $TiO_2$ 的 $2\times2\times2$ 超胞周期结构模型. 灰色,白色和黑色球形分别代表 Ti,O 和 C 原子. 数字 1-7 表示可能的 C 掺杂位,其中考虑了 7 种不同的 C-C 形貌

## 2 Results and discussion

### 2.1 Geometry

We first optimize the lattice parameters for the rutile $TiO_2$. The unit cell is tetragonal ($a = b = 4.639\ 5$ Å, $c = 2.987\ 3$ Å, space group $P42/mnm$, $D_4H_h^{14}$) and contains two Ti atoms at positions (0, 0, 0) and (1/2, 1/2, 1/2) and four O atoms at positions ($u$, $u$, 0; 1/2 + $u$, 1/2 − $u$, 1/2) with $u = \pm0.304\ 8$ in units of c. These Ti atoms are surrounded by a slightly distorted octahedron of O atoms, with a rectangular basal plane at a distance of 1.95 Å from Ti and two vertex O atoms at 1.98 Å. O atom is surrounded by three Ti.

### 2.2 Electronic and magnetic properties

Since it is unclear which state of anion-substitution by a C atom causes the ferromagnetism in the $TiO_2$, we start a single O replaced by a C (black atom numbered C in Fig. 1) atom in the $2\times2\times2$ supercell, corresponding

to a doping concentration of 3.125 at.%. We find that the calculated total energy of doping at $C_O$ with spin polarization is about 30 meV lower than the non-spin-polarized case. This means $C_O$ favors the spin-polarized state in rutile $TiO_2$. However, the predicted magnetic moment is only about 0.06 $\mu_B$ per C. The magnetic moment mainly comes from the *p* orbitals of C when it substitutes O in the rutile host.

Figure 2 presents the electronic densities of states (DOS) of the undoped $TiO_2$, and the site-projected DOS of the C 2*s*2*p*, O 2*s*2*p*, and Ti 4*s*3*d*, respectively. Compared to the undoped $TiO_2$, the C doped one leads to new impurity bands localized in the bandgap of the matrix. It seems to come mainly from the p-state of C and the d-state of Ti. The Fermi level ($E_F$) is located at the top of the impurity bands. The sample is an insulator.

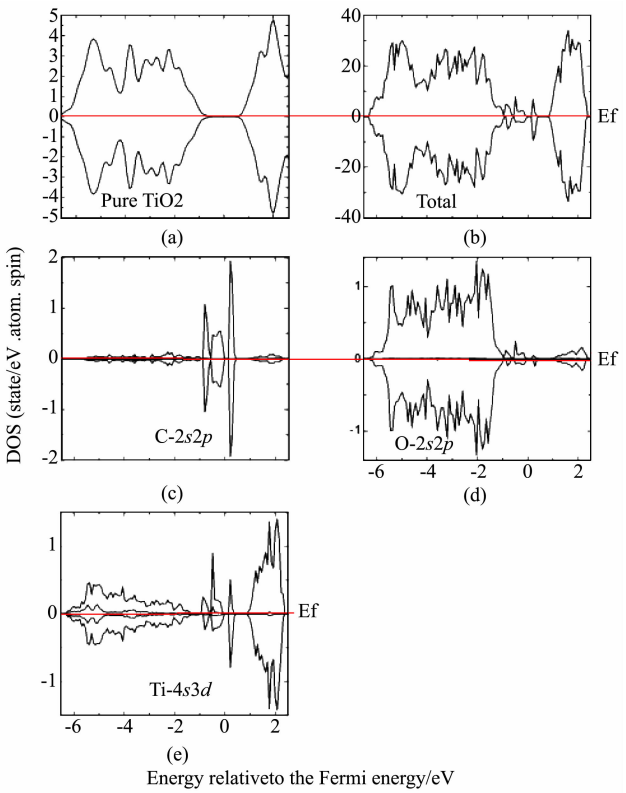


Fig. 2 (a) Total DOS for pure rutile $TiO_2$, and (b) spin polarized DOS for single C-doped rutile $Ti_{16}O_{31}C$. (c), (d) and (e) give partial spin polarized DOS for the C 2*s* and 2*p*, O 2*s* and 2*p*, and Ti 4*s* and 3*d* states, respectively. The *s* DOSs is denoted by the black shadow areas. Positive DOS represent the majority spin, while negative DOS represent the minority spin. The Fermi level (Ef in red color) has been shifted to 0 eV.
图 2 (a) 金红石结构 $TiO_2$ 的总能态密度图,和(b) 单个 C 原子掺杂的 $Ti_{16}O_{31}C$ 的自旋极化能态密度图. (c), (d) 和 (e) 分别给出了 C 2*s* 和 2*p*,O 2*s* 和 2*p* 以及 Ti 4*s* 和 3*d* 的自旋极化分态态密度图. *s* 态的能态密度图为图中的黑色阴影面积. 正的能态密度代表多数自旋极化态,负的能态密度代表少数自旋极化态. 费米能级已经归零.

Figure 3 shows the total valence charge density and spin density contour plots for $Ti_{16}O_{31}C_1$. As can be seen, the spin density is concentrated mostly to the vicinity of the C dopant itself and its neighboring Ti and O atoms, and the main moments in the supercell originate from them, consistent with Fig. 2.

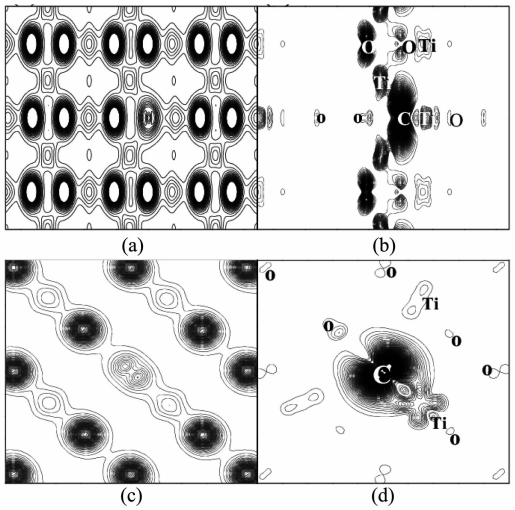


Fig. 3 Valence charge density (left column) and spin density (right column) distributions of the C-doped rutile $Ti_{16}O_{31}C$. The top panels (a), (b): in the (1-10) plane. The bottom panels (c), (d): in the (001) plane
图 3 单个 C 原子掺杂的 $Ti_{16}O_{31}C$ 的电荷密度图(左)和自旋密度图(右). 上面两图(a), (b):在 (1-10) 平面内, 下面两图 (c), (d): 在(001)平面内

As we all know, the magnetic interaction between two dopant atoms plays a key role in the magnetic properties of the system. In order to determine its stable magnetic ground state, it needs to perform the total energies calculation of the FM and antiferromagnetic (AFM) phases in C-doped $TiO_2$. To gain the deeper insight into the magnetic coupling between two C atoms, we have substituted one more O atom by C atom in $TiO_2$. The average doping concentration density in the supercell is about 6.25 at.%, the evolution of the ferromagnetism as a function of the doping concentration sites of C can be accordingly studied. We varied the positions of the second C atom with respect to the first one (Fig. 1, numbered Co), to investigate the dependency of the magnetic coupling on the interatomic distance, bond angles and coordinates. We have considered seven different relative C-C configurations, as shown in Fig. 1. Configurations I-III correspond to the replacements of two (I, II, and III are not two!) nearest-neighboring O atoms by C on the rectangular basal plane, configuration IV corresponds to the replacement of the second O atom by C on the vertex site. These correspond to sites 1, 2, 3 and 4 in Fig. 1. Configurations V-VII are to replace the fourth nearest-neighboring O atoms by C. They correspond to sites 5, 6, and 7 in Fig. 1. For each configuration, we study the total energies of the $Ti_{16}O_{30}C_2$ supercell by allowing C atoms to couple FM ($\uparrow\uparrow$) as well as AFM ($\uparrow\downarrow$), where the signs $\uparrow\uparrow$ and $\uparrow\downarrow$ denote the spins align parallel or antiparallel. The magnetic coupling is determined by the total energies difference $\Delta E$ of the supercell between spin configurations $\uparrow\uparrow$ and $\uparrow\downarrow$. The calcu-

lated results are summarized in Table 1. Only configurations I-III, with two C atoms close together, show FM. As the distance between two C atoms is the shortest, the magnetic coupling is the strongest (configuration II) However, configuration IV is nonmagnetic, i. e., the FM and AFM states are degenerated. This may be caused by the 90° C-Ti-C bond, where the *p* orbitals spatial distributions of the two C atoms have no interaction, they can orient independently. The results have been confirmed by the formation energy calculation using equation: $E(\text{form}) = E(Ti_{16}O_{30}C_2) - E(Ti_{16}O_{32}) - 2\mu(C) + 2\mu(O)$. The difference of the magnetic moment per C at different sites may be caused by the local chemical environment.

**Table 1 The second column gives the different configurations between two C atoms in $Ti_{16}O_{30}C_2$. The *d* is the separation between two C atoms before structure relaxation. The ΔE is the total energy difference between the FM and AFM orders in each supercell. This total energy difference has been used to characterize the FM magnetic coupling, given in column 5. The last column gives the induced magnetic moment on each C**

**表1 第二列给出了 $Ti_{16}O_{30}C_2$ 中两个C原子之间不同的掺杂形貌. *d* 表示结构驰豫前两个C原子之间的距离. Δ*E* 表示铁磁态和反铁磁态之间的总能差. 第五列表示用这个总能差来表征磁耦合类别. 最后一列表示每个C原子的磁矩大小**

| Geometry | Configurations | $d_{C-C}$/Å | Δ*E*/meV | Coupling | $\mu_B$ per C |
|---|---|---|---|---|---|
| Rutile | I (C, 1) | 2.988 | -11.0 | FM | 0.6 |
| | II (C, 2) | 2.562 | -71.7 | FM | 1.3 |
| | III (C, 3) | 3.936 | -11.5 | FM | 1.4 |
| | IV (C, 4) | 2.806 | 0.0 | — | 0.0 |
| | V (C, 5) | 6.561 | 2.3 | AFM | 0.0 |
| | VI (C, 6) | 7.210 | 0.1 | — | 0.0 |
| | VII (C, 7) | 6.522 | 0.1 | — | 0.0 |

As is well known, the C dopant is very different from the 3*d* dopants. For further illustrating the ferromagnetism of $Ti_{16}O_{30}C_2$, Fig. 4 presents the electronic densities of states (DOS) of configuration II. From the total DOS of $Ti_{16}O_{30}C_2$ and the site-projected DOS of the C 2*s* and 2*p*, O 2*s* and 2*p*, and Ti 4*s* and 3*d*, we can see that the C doping leads to some new features: (i) There is a strong peak at the Fermi energy in the total DOS; (ii) the shift of the Fermi level ($E_F$), which appears to be placed in the region of this 2*p*-like impurity band because the number of electrons in the unit-cell changes and (iii) the splitting of the impurity band into two spin-resolved bands. As a result, the $Ti_{16}O_{30}C_2$ acquires magnetization. Due to C doping, the rutile $TiO_2$ becomes magnetic pseudo-metal, where the $E_F$ goes into valence band in the spin-up channel, while the spin-down levels show a few DOS near $E_F$. Recently, Bannikov *et al* have reported the spin polarization induced by replacement of O atoms by 2*p* impurities (B, C and N) in nonmagnetic cubic $SrMO_3$ (M = Ti, Zr and Sn) perovskite[27]. They have shown the half-metallic picture for $SrZrO_2.875C_0.125$ that the main contribution into DOS at $E_F$ is provided by C 2*p* states and by 2*p* states of O atoms near to the impurity.

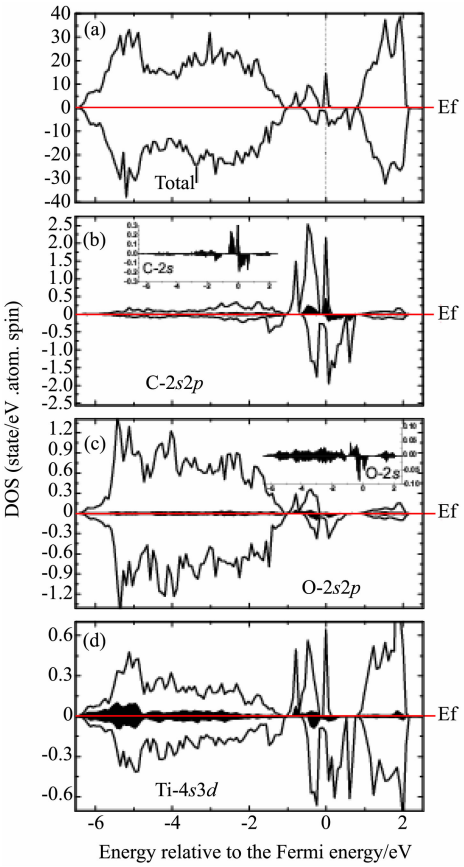


Fig. 4 (a) Total spin polarized DOS for C-doped rutile $TiO_2$. (b), (c) and (d) give partial spin polarized DOS for the C 2*s* and 2*p*, O 2*s* and 2*p*, and Ti 4*s* and 3*d* states, respectively. The *s* DOSs is denoted by the black shadow areas. Positive DOS represent the majority spin, while negative DOS represent the minority spin. The Fermi level (Ef in red color) has been shifted to 0 eV. The illustrations in (b) and (c) are amplified for C-2*s* and O-2*s*, respectively

图4 (a) 单个C原子掺杂的 $Ti_{16}O_{31}C$ 的自旋极化能态密度图. (b), (c) 和 (d) 分别给出了C 2*s* 和 2*p*, O 2*s* 和 2*p* 以及 Ti 4*s* 和 3*d* 的自旋极化分态态密度图. *s* 态的能态密度图为图中的黑色阴影面积. 正的能态密度代表多数自旋极化态, 负的能态密度代表少数自旋极化态. 费米能级已经归零. 图(b) 和 (c) 中的内嵌图分别为放大的 C-2*s* 和 O-2*s* 的能态密度图

From Fig. 4, the C 2*s* and 2*p* DOSs are both with a rather large exchange splitting between majority and minority spin states. As far as the O 2*s*, 2*p* and the Ti 4*s*, 3*d* site-projected partial DOSs are concerned, they also deviate appreciably from the pure behavior of them. It is noting that the C 2*s*, 2*p* states hybridize strongly with the O 2*s*, 2*p* and Ti 4*s*, 3*d* states near $E_F$, indicating a strong interaction between both of them. The spin-up bands are almost fully occupied while the spin-down bands are partially filled, resulting in a magnetic moment of 1.3 $\mu_B$ per C in rutile structure. The relatively large

width of the DOS comes mainly from the defect states and the strong mixing with the O 2*p* and Ti 3d levels allowed the DOS plots. Compared to *s* states, the O 2*p*, C 2*p*, and Ti 3*d* states have larger amplitude at $E_F$. In a covalent picture, the hybridization forms the bonding and antibonding states. The bonding states are occupied. The antibonding states can be higher in energy than the nonbonding states. According to the Ref. 21, the interaction follows essentially from quantum mechanical level repulsion, which "pushes" the minority state upward, crossing the $E_F$. Consequently, the *p* states are split into more stable threefold $t_2$ states.

One might at this point want to know what mechanism is responsible for the ferromagnetism of C-doped $TiO_2$. Obviously, the well known DMSs theory is unsuitable. There are unpaired spins in 3*d* and 4*f* orbitals, but there are no such orbitals in $Ti_{16}O_{30}C_2$. Pan *et al* have suggested the Zn-C coupling as the origin of magnetism in C-doped ZnO[20], but they have not taken the O 2*s*, 2*p* states into consideration. Later, Shen *et al* have studied the ferromagnetism in 2*p* element-doped II-oxide and III-nitride semiconductors[21]. They attribute the FM to a *p-d* exchange-like *p-p* coupling interaction, deriving from the similar symmetry and wave function between the impurity (*p*-like $t_{2g}$) and valence (*p*) states. Similarly, Bannikov *et al* have attributed the magnetism in $SrZrO_{2.875}C_{0.125}$ system to the spin polarization of the C atoms and the O atoms in the second coordination sphere of the C, while the nearest-neighboring metallic atoms of the impurity still remain non-magnetic[23]. In Fig. 4, however, the nearest-neighboring Ti atoms of the C are not non-magnetic anymore in $Ti_{16}O_{30}C_2$. The C 2*s*, 2*p* states overlap heavily both with the O 2*s*, 2*p* and the Ti 4*s*, 3*d* states near $E_F$. Thus, a simple conclusion can not be given on which interaction (the interaction between the C 2*s*, 2*p* and the Ti 4*s*, 3*d* states, or the interaction between the C 2*s*, 2*p* and the O 2*s*, 2*p* states) is responsible for the ferromagnetism of C-doped $TiO_2$. The presented magnetization picture differs from that of the simple oxides and the 3*d* element-doped semiconductors. In oxides, the induced moments are located on neighboring cations of the impurity, while O atoms in the second coordination sphere do not acquire spin polarization[23]. In 3*d* element-doped wurtzite host semiconductors, the spin is exclusively localized in a tetrahedron formed by the four nearest-neighboring anions of the 3*d* impurity[21]. However, in rutile $Ti_{16}O_{30}C_2$ shown in Fig. 4, the *p-d* hybridization and *p-p* coupling both contribute to the magnetism of $Ti_{16}O_{30}C_2$. The induced magnetization at 3*d* orbitals of Ti and 2*p* orbitals of O give about 23.5 % (0.503) and 15.2 % (0.325) of the total magnetization, respectively. The wave function of the C 2*p* states spatially extend to the neighboring Ti 3*d* states, hybridize with them. This *p-d* exchange hybridization, lead to the spin alignment of parent C atoms, give a contribution to the FM coupling of the system. Simultaneously, the electrons in *p* states are more delocalized than those in *d* and *f* states, which could promote long range exchange interactions[21]. The symmetry and the wave function (*p*-like $t_{2g}$) of the impurity 2*p* state are similar to that of the top valence band of the III-nitride and II-oxide, which consists mostly of anion *p* orbitals. Therefore, a strong *p-p* coupling interaction between the impurity and valence band states is allowed near the $E_F$. As is well known, the substitution of C for O in $TiO_2$ introduces impurity moments as well as holes. The strong *p-p* coupling interaction leads to the strong coupling between the impurity and carrier spin orientations. Sufficiently the dense spin polarized carriers are able to effectively mediate an indirect FM coupling between the 2*p* dopants. In other words, a *p-d* exchange-like *p-p* coupling interaction mechanism also works. The interaction is long range in FM DMSs, due to the extended valence hole states. In conclusion, the mechanisms responsible for the FM properties of C-doped $TiO_2$ are the collective effects from a *p-d* exchange-like *p-p* coupling interaction and a *p-d* exchange hybridization, consistent with the mechanism proposed by Zainullina et al.[16]. Thus, the $Ti_{16}O_{30}C_2$ gives significant ferromagnetism.

Figure 5 shows the total valence charge density and spin density contour plots for $Ti_{16}O_{30}C_2$. As can be seen, the spin density is concentrated mostly to the vicinity of the C dopant itself and its neighboring Ti and O atoms, and the main moments in the supercell originate from them, consistent with Fig. 4. The impurity gives rise to the spin polarization of both Ti and O atoms near the C impurity. The result indicates the strong spin-polarized hybridization between C 2*s*, 2*p* and O 2*s*, 2*p* and Ti 4*s*, 3*d* states, the FM in $Ti_{16}O_{30}C_2$ originates from both of them. Moreover, the spatial distribution of spin charge density from O atoms reveals its *p* character. Different from Mn ions in GaAs:Mn which polarizes spin of holes in opposite direction, the spin density near each anion impurity in 2*p* element-doped DMSs tends to align parallel to the moment of the impurity ion under *p-p* interaction. It is thought to be a signature of the long range *p-p* coupling interaction as one of the origin of FM in C-doped $TiO_2$. It is also suggested that the magnetic interaction between the dopant C 2*p* and the anion O 2*p* states can lower the total energy, therefore stabilizing the FM alignment between C atoms.

## 3 Conclusions

In summary, using first-principles calculations, we have shown that the 2*p* element C-doped rutile $TiO_2$ has FM characteristics. The C dopants tend to couple ferromagnetically around the Ti atom in the rutile structure. The spin charge density is concentrated mostly to the vicinity of the C dopant itself and its neighboring Ti and O atoms. We propose that the mechanisms responsible for the FM properties in C-doped $TiO_2$ are the collective effects from a *p-d* exchange-like *p-p* coupling interaction and *p-d* exchange hybridization. Thus, the C-doped $TiO_2$ gives significant ferromagnetism. The *p-d* exchange-like *p-p* coupling interaction is derived from the similar symmetry and wave function between the impurity (*p*-like $t_{2g}$) and valence (*p*) states. This magnetic interaction is long range.

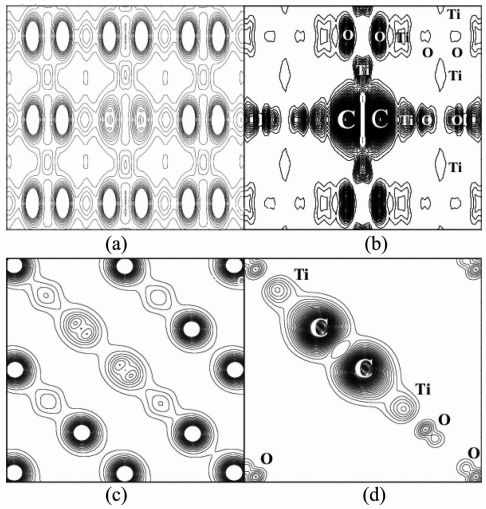


Fig. 5 Valence charge density (left column) and spin density (right column) distributions of the C-doped rutile $TiO_2$. The top panels (a), (b): in the (1-10) plane. The bottom panels (c), (d): in the (001) plane
图5 两个C原子掺杂的$TiO_2$的电荷密度图(左)和自旋密度图(右). 上面两图(a), (b):在(1-10)平面内, 下面两图(c), (d): 在(001)平面内

## Acknowledgments

This work was supported in part by the National Natural Science Foundation of China (11104299 and 61006090), the Fund of Shanghai Science and Technology Foundation (16ZR1447400). Computational support from Shanghai Super-computer Center is acknowledged. Work at UC Davis is supported by US National Science Foundation with grant No. ECCS-1232275.

## References

[1] Shan G B, Demopoulos G P. Near-infrared sunlight harvesting in dye-sensitized solar cells via the insertion of an upconverter-$TiO_2$ nanocomposite layer [J]. *Adv. Mater.* 2010, **22**: 4373.
[2] Takeshita K, Yamakata A, Ishibashi T, *et al.* Transient IR absorption study of charge carriers photogenerated in sulfur-doped $TiO_2$ [J]. *J Photochem Phytobiol A: Chem.* 2006, **177**: 269 - 75.
[3] Ratanatawanate C, Xiong C R, Balkus K J. Fabrication of PbS quantum dot doped $TiO_2$ nanotubes [J]. *ACS Nano.* 2008, **2**: 1682 - 1688.
[4] Janisch R, Gopal P, Spaldin N A, Transition metal-doped $TiO_2$ and ZnO—present status of the field [J]. *J. Phys.: Condens. Matter.* 2005, **17**: R657.
[5] Mallia G, Harrison N M. Magnetic moment and coupling mechanism of iron-doped rutile $TiO_2$ from first principles [J]. *Phys. Rev.* B, 2007, **75**: 165201.
[6] Hu S J, Yan S S, Yao X X, *et al.* Electronic structure and magnetic properties of Fe0. 125Sn0. 8752 [J]. *Phys. Rev. B*, 2007, **75**: 094412.
[7] Komen C V, Thurber A, Reddy K M, *et al.* Structure-magnetic property relationship in transition metal (M = V, Cr, Mn, Fe, Co, Ni) (M = V, Cr, Mn, Fe, Co, Ni) doped $SnO_2SnO_2$ nanoparticles [J]. *J. Appl. Phys.* 2008, **103**: 07D141.
[8] Philip J, Punnoose A, Kim B I, *et al.* Carrier-controlled ferromagnetism in transparent oxide semiconductors [J]. *Nat. Mter.* 2006, **5**: 298.
[9] Coey J M D, Venkatesan M, Stamenov P, *et al.* Magnetism in hafnium dioxide [J]. *Phys. Rev. B*, 2005, **72**: 024450.
[10] Bai H L, He S M, Shuai X T, Ferromagnetism, variable range hopping and anomalous Hall effect in epitaxial Co:ZnO thin film [J]. *Chin. Phys.* B. 2012, **21**: 107201.
[11] Dai Y Y, Yan S S, Tian Y F, *et al.* Universal spin-dependent variable range hopping in wide-band-gap oxide ferromagnetic semiconductors [J]. *Chin. Phys. B*, 2010, **19**(3):037203.
[12] Jia C W, Xie E Q, Zhao J G, *et al.* Visible and near-infrared photoluminescences of europium-doped titania film [J]. *J. Appl. Phys.* 2006, **100**: 023529.
[13] Komuro S, Katsumata T, Kokai H, *et al.* Change in photoluminescence from Er-doped $TiO_2$ thin films induced by optically assisted reduction[J]. *Appl. Phys. Lett.* 2002, **81**: 4733.
[14] Gao H T, Ding C H, Dai D M, Density functional characterization of C-doped anatase $TiO_2$ with different oxidation state [J]. *Journal of Molecular Structure: THEOCHEM*, 2010, **944**: 156 - 162.
[15] Tian F H, Liu C B, Zhang D J, *et al.* On the Origin of the Visible-Light Activity of Titanium Dioxide Doped with Carbonate Species [J]. Chem. Phys. Chem 2010, **11**: 3269 - 3272.
[16] Wang P, Liu Z R, Lin F, *et al.* Optimizing photoelectrochemical properties of $TiO_2$ by chemical codoping [J]. *Phys. Rev.* B 2010, **82**: 193103.
[17] Zhang R H, Wang Q, Li Q, *et al.* First-principle calculations on optical properties of C-N-doped and C-N-codoped anatase $TiO_2$ [J]. *Physica B*, 2011, **406**: 3417 - 3422.
[18] Zainullina V M, Zhukov V P, Korotin M A, *et al.* Effect of doping by boron, carbon, and nitrogen atoms on the magnetic and photocatalytic properties of anatase [J]. *Physics of the Solid State*, 2011, **53**(7): 1353 - 1361.
[19] Long R, English N G. Density functional theory studies of doping in titania [J]. *Molecular Simulation* 36, *Nos.* 2010, 7-8: 618 - 632.
[20] Yu Z, Li X, Long X, *et al.* The study of a new n/p tunnel recombination junction and its application in a-Si:H/μc-Si:H tandem solar cells [J]. *Chin. Phys. B.* 2009, **18**: 1674 - 1678.
[21] Sedkya A, El-Suheel E. Structural and electronic characteristics of pure and doped ZnO varistors [J]. *Chin. Phys. B*, 2012, **21**(11): 116103.
[22] Duhalde S, Vignolo M F, Golmar F, *et al.* Appearance of room-temperature ferromagnetism in Cu-doped $TiO_2$-delta films [J]. *Phys. Rev. B*, 2005, **72**: 161313.
[23] Elfimov I S, Rusydi A, Csiszar S I, *et al.* Magnetizing oxides by substituting nitrogen for oxygen [J]. *Phys. Rev. Lett.* 2007, **98**: 137202.
[24] Pan H, Yi J B, Shen L, *et al.* Room-temperature ferromagnetism in carbon-doped ZnO[J]. *Phys. Rev. Lett.* 2007, **99**:127201.
[25] Shen L, Wu R Q, Pan H, *et al.* Mechanism of ferromagnetism in nitrogen-doped ZnO: First-principle calculations [J]. *Phys. Rev. B.* 2008, **78**:073306.
[26] Yu C F, Lin T J, Sun S J, *et al.* Origin of ferromagnetism in nitrogen embedded ZnO: N thin films [J]. *J Phys D: Appl. Phys.* 2007, **40**: 6497.
[27] Bannikov V V, I. R. Shein I R, V. L. Kozhevnikov V L, *et al.* Magnetism without magnetic ions in non-magnetic perovskites SrTiO3, SrZrO3 and SrSnO3 [J]. *J. Magn. Magn. Mater.* 2008, **320**: 936.
[28] Wu R Q, Liu L, Peng G W, *et al.* Magnetism in BN nanotubes induced by carbon doping [J]. *Appl. Phys. Lett.* 2005, **86**:122510.
[29] Ohldag H, Tyliszczak T, Höhne R, *et al.* pi-Electron ferromagnetism in metal-free carbon probed by soft x-ray dichroism [J]. *Phys. Rev. Lett.* 2007, **98**:187204.
[30] Blöchl P E, Projector augmented-wave method[J]. *Phys. Rev. B.* 1994, **50**: 17953.
[31] Kresse G, Furtmüller J, Efficient iterative schemes for ab initio total-energy calculations using a plane-wave basis set [J]. *Phys. Rev. B*, 1996, **54**: 11169.
[32] Perdew J P, Burke K, Ernzerhof M. Generalized gradient approximation made simple [J]. *Phys. Rev. Lett.* 1996, **77**: 3865.
[33] Monkhorst H J, Pack J D, Special points for brillouin - zone integrations [J]. *Phys. Rev. B.* 1976, **13**: 5188.